

Article

Intelligent Reflecting Surface Aided Wireless Systems with Imperfect Hardware

Nhan Duc Nguyen ¹, Anh-Tu Le ^{2,*} , Munyaradzi Munochiveyi ³ , Fatemeh Afghah ⁴  and Evangelos Pallis ⁵¹ Faculty of Engineering, Van Lang University, Ho Chi Minh City 700000, Vietnam; nhan.nd@vlu.edu.vn² Faculty of Electronics Technology, Industrial University of Ho Chi Minh City, Ho Chi Minh City 700000, Vietnam³ Department of Electrical and Electronics Engineering, University of Zimbabwe, Mount Pleasant, Harare MP167, Zimbabwe; mmunochiveyi@eng.uz.ac.zw⁴ Electrical and Computer Engineering Department, Clemson University, Clemson, SC 29634, USA; fafghah@clemson.edu⁵ Electrical and Computer Engineering, Hellenic Mediterranean University, 71004 Heraklion, Crete, Greece; pallis@pasiphae.eu

* Correspondence: leanhtu@iuh.edu.vn

Abstract: In this article, we investigate the design of reconfigurable intelligent surface (RIS)-aided transmission as a smart method to reflect signals received from access points to users and, hence, improving users' performance. To implement smart Internet of Things (IoT) networks, massive connectivity and low-cost deployment are essential in designing such systems. In particular, we consider two practical scenarios (dual-hop and single-hop transmissions). These scenarios highlight the potential of RIS in enhancing the system's outage probability performance. Furthermore, to characterize channel conditions in practice, we pay particular attention to two-channel distributions that are non-central chi-square (NCCS) distributions that approximate the channel distribution of the RIS-aided wireless system and the squared K_G distribution. In addition, the RIS-aided system may face imperfect hardware-related issues in practice. Therefore, we need to consider the degraded performance of practical RIS-aided systems by considering the detrimental impact of in-phase and quadrature-phase imbalance (IQI). To characterize the main system performance metric, we provide closed-form formulas of outage probability and ergodic capacity. We then evaluate system performance under the impacts of signal-to-noise ratio (SNR), the number of meta-surfaces, and channel parameters. All closed-form outage expressions are validated via Monte Carlo simulations. Simulation results indicate that the considered RIS scheme at dual-hop and single hop under the impact of IQI and RIS hardware impairment achieves significant improvements in terms of outage probability at high SNR and high meta-surface number N . Additionally, the simulation results demonstrate that the impact of IQI on the proposed system is limited. It is worth noting that, in terms of ergodic capacity, ergodic capacity faces an upper limit. Despite this limitation, the proposed system can still work well once some parameters are controlled well, such as the transmit SNR, levels of IQI, and the number of RIS components.

Keywords: reconfigurable intelligent surface (RIS); outage probability; in-phase and quadrature-phase imbalance (IQI)



Citation: Nguyen, N.D.; Le, A.-T.; Munochiveyi, M.; Afghah, F.; Pallis, E. Intelligent Reflecting Surface Aided Wireless Systems with Imperfect Hardware. *Electronics* **2022**, *11*, 900. <https://doi.org/10.3390/electronics11060900>

Academic Editor: Reza K. Amineh

Received: 29 December 2021

Accepted: 11 March 2022

Published: 14 March 2022

Publisher's Note: MDPI stays neutral with regard to jurisdictional claims in published maps and institutional affiliations.



Copyright: © 2022 by the authors. Licensee MDPI, Basel, Switzerland. This article is an open access article distributed under the terms and conditions of the Creative Commons Attribution (CC BY) license (<https://creativecommons.org/licenses/by/4.0/>).

1. Introduction

Recently, the emerging advances of reconfigurable intelligent surfaces (RIS) have become attractive to researchers due to their appealing ability to intelligently manipulate the propagation of electromagnetic waves [1–3]. Regarding the architecture of RIS, it has a massive integration of passive and reflecting components that can independently tune the amplitude and phase of the signal and then reflect the adjusted signal. The operation

of RIS is similar to that of full-duplex relays. Compared to the traditional relaying techniques [4,5], RIS has two main benefits. Firstly, RIS consumes much less energy during reflection due to its operation as a passive device, thus avoiding power-hungry radio frequency processing. Secondly, one can install RIS on a thin and lightweight film. For example, RIS enables previously uncontrollable communication participants to assist in the transmission collaboratively since it can be placed on various objects such as building facades, walls, ceilings, street signs, and advertisement boards [6]. Furthermore, system improvements can be achieved based on the reflection pattern of the RIS as reported in [7–9].

The authors in [10] have shown that multiple base stations (BSs) precoders can be jointly designed with the RIS elements in a downlink multi-cell scenario. Hence, all cell-edge users can have improved weight sum rates, while the RIS-assisted multi-cell multiple-input single-output (MISO) system was explored in [11] to maximize benefits of a RIS deployed in a network consisting of several multi-antenna base stations (BSs). Here, RIS assists the wireless transmission and suppresses the inter-cell interference faced by the single-antenna user. To achieve the maximization of the minimum weighted received signal-to-interference-plus-noise ratio (SINR) at users, the coordinated transmit beamforming at the BSs and the reflective beamforming at RIS are jointly optimized while satisfying reflection constraints at the RIS and the individual maximum transmit power constraints at BSs. By considering energy harvesting and power consumption (due to the reflecting elements' phase shift) at RIS, the authors in [12] presented the optimization of the sum-rate of a downlink MISO system with self-sustainable RIS. The study in [13] confirmed that the minimal rate of cell-edge users in a RIS-aided system can be significantly enhanced by exploiting cooperative beamforming in joint processing coordinated multipoint downlink transmission. The authors in [14,15] deployed a simultaneous wireless information and power transfer (SWIPT) approach to allow a joint RIS design and optimization of transmit beamforming in a downlink. For their main result, the authors demonstrated that RIS guarantees quality-of-service (QoS) requirements and optimal total power consumption in RIS-aided SWIPT networks. Furthermore, in other scenarios, RIS has also been proved as a promising technique to benefit wireless networks. For instance, RIS-aided systems improved performance in the recent studies of [16–22], where RIS is utilized together with unmanned aerial vehicles (UAVs), non-orthogonal multiple access (NOMA), backscatter communication, physical layer security, cognitive radio (CR), and mobile edge computing (MEC). However, all the above works have not focused on the characteristics of channels; hence, this motivates our investigation on the impact of non-central chi-square (NCCS) distribution and squared K_G distribution on RIS-aided wireless systems. The NCCS and K_G distributions approximate the likely channel distribution of RIS-aided wireless systems.

1.1. Related Studies

In other perspectives, ref. [23] analyzed the asymptotic performance of the large-scale MISO downlink system relying on spatial correlation statistics. The authors in [24,25] considered imperfect channel state information (CSI) using discrete-resolution RIS to boost weighted sum-rate for downlink MISO users. The works in [26,27] examined imperfect CSIs in robust beamforming design that results in less power consumption. To achieve low-overhead channel estimation, several works [28–30] have studied RIS reflection patterns and designed pilot sequences. The error probability of RIS-enabled systems is studied with quantized channel phase compensation in [31]. The authors provided analysis of exact and asymptotic bit error rate (BER) expressions in different practical channel scenarios and the existence of the direct link.

Moreover in terms of mobility, refs. [32,33] proposed novel RIS-aided wireless communication channel estimation schemes in mobility scenarios. Specifically, in [32], the authors proposed a channel estimation scheme for RIS-aided systems in mobility scenarios. The authors exploited Kalman filters to take advantage of the channel time correlation. Furthermore, the cascaded RIS channel is represented as a state-space model based on the mobility

scenario. The optimal RIS reflection coefficients are then obtained via minimum mean square error (MMSE). Differently, in [33], the authors proposed two wide-band channel estimation frameworks integrating multi-path and single-path Doppler shift adjustments.

Several recent research works have also studied the application of machine learning in RIS channel estimation. In [34], the authors studied the protection of users' location data during RIS-enhanced millimeter wave (mmWave) channel estimation by incorporating privacy-preserving federated learning. Ref. [35] proposed two residual neural network algorithms—single-scale enhanced deep residual (EDSR) and multi-scale enhanced deep residual (MDSR)—to obtain accurate CSI in a semi-passive RIS assisted network. The RIS device is equipped with a small number of active radio frequency units for capturing partial CSI. Similarly, in [36], the authors also proposed three residual neural networks—blind convolutional denoising network, convolutional denoising generative adversarial networks, and multiple residual dense networks—to obtain accurate CSI. In [37], the authors introduced an artificial intelligence-assisted channel estimation scheme in RIS-enabled networks. Furthermore, in [38], the authors explored a deep learning approach to obtain an achievable rate by studying RIS phase shifts and receiver location interaction without utilizing CSI. Once the model is trained adequately, the deep learning model can be used to predict the optimal number of RIS elements for any receiver location.

In terms of RIS-assisted multiple-input multiple-output (MIMO) networks, the authors in [39] proposed a joint precoding and RIS phase adjustment design for RIS-assisted MIMO systems. Then, in [7], the authors examined information exchange and passive beamforming for RIS-aided multi-user MIMO networks. The authors designed a stochastic algorithm to solve the bilinear receiver estimation problem. Similarly, in [40], the authors designed RIS phase shifts in a RIS-assisted massive MIMO network with direct links based on the statistical CSI. Then, the authors derived the uplink ergodic rate, and afterward, the maximized sum rate was obtained via a genetic algorithm. Differently, in [41], the authors studied the outage probability of a RIS-enabled MIMO network by exploiting Kornecker channel models to characterize MIMO antennas spatial correlations and RIS-reflecting elements. The authors utilized random matrix theory and Mellin transforms to obtain the outage probability. In [42], the authors proposed a new signal-passing-based algorithm to factorize the RIS-aided multi-user MIMO cascaded channels.

Furthermore, to improve the performance of wireless systems equipped with multiple antennas, several works have noted that RIS can improve spectrum efficiency [10,43,44] of such networks. For example, the authors in [43] studied RIS-aided single-cell systems equipped with multiple antennas. As the main result, one can reduce active RF chains. Regarding the data rate, it can be achieved with similar performance compared with the massive MIMO without RIS. The authors in [10] confirmed the improvement of cell-edge users, and inter-cell interference can be mitigated in the context of a RIS-aided multi-cell MIMO system. In [44], when the RIS is activated for both functions of wireless information and power transfer, the system can improve its performance in terms of energy harvesting.

Furthermore, in the context of millimeter-wave (mmWave) communications relying on RIS, the accurate acquisition of the CSI is important to achieve high RIS beamforming gain. Ref. [45] considered channel estimation in RIS-aided mmWave communications assuming small-scale fading. The authors characterized statistically fluctuating two-ray (FTR) distributions. Ref. [46] addressed channel estimation in high-speed railway networks relying on RIS-aided mmWave communication. The authors proposed a reinforcement-based approach combining long short-term memory (LSTM) and deep deterministic policy gradient (DDPG) to design the base station transmit beamforming and RIS phase shifts. Ref. [47] proposed an alternating direction method of multipliers (ADMM)-based channel estimation method for RIS-enabled millimeter-wave communication. Simulation results demonstrated that the proposed ADMM approach is beneficial for channel estimation and also reduces training overhead.

For other emerging RIS-aided multi-user communication systems such as RIS-UAV [48] and RIS-CR [49], novel channel estimation techniques have been proposed. In [48], the au-

thors studied the secure communication of RIS-aided UAV communication in the presence of eavesdroppers. In addition, the authors assumed that the CSI of the eavesdropper is imperfect. The authors maximized the average worst-case secrecy rate by jointly designing the trajectory of the UAV, the RIS phase shifts, and the legitimate users' transmit power. The successive convex approximation (SCA), \mathcal{S} -Procedure, and semidefinite relaxation (SDR) methods are proposed to solve the formulated non-convex problem. In [49] the authors considered maximizing the secondary user (SU) achievable rate by jointly designing SU beamforming and RIS reflecting coefficients subject to SU transmit power constraint and PU interference temperature constraint in a multiple RIS-aided MISO CR network. The network consists of a single SU coexisting with a primary network containing multiple PUs.

1.2. Motivations and Contributions

However, only a few papers considered the impact of hardware impairment of RIS-aided systems [50–53]. For example, the work in [50] examined secure communication in RIS-aided systems in the presence of transceiver hardware impairments. The optimal secrecy rate can be achieved while satisfying the transmit power condition on the base station related to the active beamforming. The authors in [51] explored a single eavesdropper in a RIS-NOMA system with hardware impairment. The study considered the physical layer security (PLS) performance of the system under the impact of hardware impairment. They derived the closed-form formula, i.e., secrecy outage probability (SOP).

To the best of our knowledge, the impact of hardware impairment limits system performance significantly. In some cases, interference needs to be mitigated in emerging systems as well as in traditional systems. In the perspective of the promising application of RIS-aided systems, it is more than important to study how the system deals with the degradation from hardware impairment. To fill the gap in existing work and motivated by aforementioned studies [51–53], we investigate the outage performance of dual-hop RIS-aided systems for promising applications in Internet-of-Thing (IoT) networks under IQI imperfect hardware. We provide Table 1 to compare findings in our work with related studies and highlight our main contributions relative to previous works.

Our main contributions can be summarized as follows:

- As first study, we emphasize on performance analysis of the representative destination user by considering a detrimental factor of in-phase and quadrature-phase imbalance (IQI). We deploy the non-central chi-square (NCCS) distribution to approximate the channel distribution of the RIS-aided wireless system. To further exhibit system performance, we also adopt a squared K_G distribution.
- To confirm the strong contribution of RIS in improving performance of distant users, we compare two possible scenarios related to the different roles of RIS in future wireless communication networks: firstly, when RIS acts as a relay in dual-hop communication (RIS-DH); and secondly, when RIS plays the role of a transmitter (RIS-T).
- Then, we focus on outage probability and average capacity for the two above-mentioned practical situations. To further provide insights into such RIS-aided systems, we derive asymptotic calculations of outage probability for both RIS-DH and RIS-T schemes.
- The main results demonstrate that, under the impact of IQI and RIS hardware impairment, the proposed dual and single hops RIS-aided scheme achieves significant improvement in terms of outage probability at high SNR and high meta-surface number N . Additionally, simulation results show that the impact of IQI on the proposed system is limited. Thus, our work provides useful guidelines for future application of RIS systems under the impact of IQI.

The rest of this paper is organized as follows based on the organization in [54,55]: Section 2 presents the system model of RIS-aided system in the presence of IQI. In Section 3, we derive the exact closed-form analytical expressions of outage probability. Section 4 provides the ergodic capacity of the system. Section 5 provides numerical simulations. Section 6 concludes the paper.

Table 1. Comparison of related works with current work.

References	System Model	Performance Analysis	Key Findings
[50]	A reconfigurable intelligent surface (RIS)-aided secure communication system.	The successive convex approximation (SCA) method is used to solve the active beamforming optimization subproblem, while the passive beamforming is obtained by using the semidefinite program (SDP) method.	The proposed transmission design scheme is more robust to the hardware impairments than the conventional non-robust scheme.
[51]	RIS-assisted NOMA technology applied in the internet of things (IoT) with a single eavesdropper.	The closed-form formula of the user's secrecy outage probability (SOP).	The main factors affecting the SOP are parameters of RIS, target rate and transmit SNR.
[52]	RIS-assisted multiple-input single-output (MISO) downlink network.	The spectral and energy efficiency.	The degraded performance at high SNR regime is confirmed to be mainly affected by hardware impairments rather than by the RIS's phase noise.
[53]	RIS assisted multiple antennas systems.	A closed-form optimal solution to the source transmit beamforming.	The proposed beamforming scheme is more robust to the imperfect hardware than that of the conventional SNR maximized approach.
Our work	Dual and single hops RIS-aided systems.	Outage Performance and average rate.	Outage performance and average rate are mostly adjusted by configuration of RIS.

2. System Model

In this paper, we consider the existence of IQI on both the TX and the RX. In general, IQI is modeled as phase and/or amplitude imbalance between the transceiver I and Q signal paths. Therefore, the time-domain baseband representation of the IQI impaired signal is represented as [56]:

$$\hat{y} = \beta_{T/R}y + \bar{\beta}_{T/R}y^*, \quad (1)$$

where y stands for the baseband transmitted signal under perfect transmitter/receiver (TX/RX) IQI matching. We denote y^* as the mirror signal after being affected by IQI. Detailed IQI coefficients $\omega_{t/r}$ and $\bar{\omega}_{t/r}$ are expressed by [57], respectively, as follows

$$\beta_T = \frac{(1 + \mu_T \exp(jv_T))}{2}, \quad (2a)$$

$$\bar{\beta}_T = \frac{(1 - \mu_T \exp(jv_T))}{2}, \quad (2b)$$

$$\beta_R = \frac{(1 + \mu_R \exp(jv_R))}{2}, \quad (2c)$$

$$\bar{\beta}_R = \frac{(1 - \mu_R \exp(jv_R))}{2}. \quad (2d)$$

where $\mu_{T/R}$ and $v_{T/R}$ are the TX/RX amplitude and phase mismatch levels, respectively. Moreover, we have $\phi_t = \phi_r = 1$ and $\phi_r = \phi_t = 0^\circ$ for ideal cases.

2.1. RIS-DH Scheme

In this case, we consider RIS-aided communication with an access point (S), a RIS that is composed of N reflecting meta-surfaces, a destination (D), and S and D are equipped

single antenna as shown in Figure 1. Moreover, we assume link S to D does not exist [58]. Thus, the signal at D is given as follows

$$y_D = \beta_D \left[\sqrt{P_S} \sum_{n=1}^N f_{R,n} f_{D,n} g_n (\beta_S x + \bar{\beta}_S(x)^*) + n_0 \right] + \bar{\beta}_D \left[\sqrt{P_S} \sum_{n=1}^N f_{R,n} f_{D,n} g_n (\beta_S x + \bar{\beta}_S(x)^*) + n_0 \right]^* \tag{3}$$

where x is the transmitted symbol; P_S is the transmit power at S; n_D is the additive white Gaussian noise (AWGN) with $CN(0, N_0)$; $g_n = \Theta e^{j\phi_n}$ is the reflection coefficient produced by the n th reflector of the RIS; $\Theta = 1$ is the ideal phase shifts; β_S and $\bar{\beta}_S$ denote the amplitude and phase parameters of the IQI at S, respectively; β_D and $\bar{\beta}_D$ are defined as the amplitude and phase parameters of the IQI at D; $f_{R,n}$ and $f_{D,n}$ are the channel gains with $f_{R,n} = d_1^{-\frac{\chi}{2}} h_{R,n} e^{-j\theta_n}$, $f_{D,n} = d_2^{-\frac{\chi}{2}} h_{D,n} e^{-j\varphi_n}$, where d_1 and d_2 are the distances from S to RIS and RIS to D, respectively; χ denotes the path loss coefficient; $h_{R,n}$ and $h_{D,n}$ are the amplitudes of channel and following independent distributed Rayleigh random variables (RVs); and θ_n and φ_n are the phases of the channel gains. Hence, we compute SNR at D as follows [59]:

$$\gamma_D = \frac{P_S \left| \sum_{n=1}^N h_{R,n} h_{D,n} e^{j\phi_n - j\theta_n - j\varphi_n} \right|^2 \omega_1}{P_S \left| \sum_{n=1}^N h_{R,n} h_{D,n} e^{j\phi_n - j\theta_n - j\varphi_n} \right|^2 \omega_2 + d_1^\chi d_2^\chi N_0 \omega_3} \tag{4}$$

where $\omega_1 = |\beta_D \beta_S + \bar{\beta}_D \bar{\beta}_S^*|^2$, $\omega_2 = |\beta_D \bar{\beta}_S + \bar{\beta}_D \beta_S^*|^2$ and $\omega_3 = |\beta_D|^2 + |\bar{\beta}_D|^2$. Based on [57], we can approximate $\omega_1 \approx |\beta_D \beta_S|^2 + |\bar{\beta}_D \bar{\beta}_S^*|^2$ and $\omega_2 \approx |\beta_D \bar{\beta}_S|^2 + |\bar{\beta}_D \beta_S^*|^2$. Next, we set $\phi_n = \theta_n + \varphi_n$ as [59]. Then, the maximum amount of γ_D is given as follows:

$$\begin{aligned} \gamma_D &= \frac{P_S \left[\sum_{n=1}^N h_{R,n} h_{D,n} \right]^2 \omega_1}{P_S \left[\sum_{n=1}^N h_{R,n} h_{D,n} \right]^2 \omega_2 + d_1^\chi d_2^\chi N_0 \omega_3} \\ &= \frac{\eta \omega_1}{\eta \omega_2 + \omega_3} \end{aligned} \tag{5}$$

where $\rho_S = \frac{P_S}{N_0}$ denotes the average SNR, $Z = \sum_{n=1}^N h_{R,n} h_{D,n}$, and $\eta = \frac{\rho_S}{d_1^\chi d_2^\chi} Z^2$.

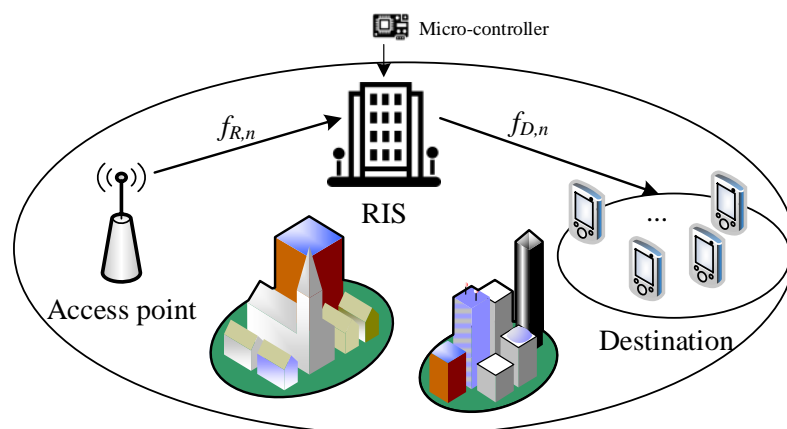


Figure 1. System model for the proposed RIS-aided dual-hop communication scheme.

The above-derived SINR expressions are necessary to compute other main system performance metrics. It is worth noting that the transmit SNR plays an influential role in varying performance at destinations. However, the system needs to adjust parameters at the transmit side, for example, the transmit SNR, so as to achieve the expected performance. We will present the closed-form expression to illustrate performance in terms of outage probability and ergodic capacity in Sections 3 and 4.

2.2. RIS-T Scheme

In this case, we consider an RF signal generator, a RIS with N reflecting meta-surfaces, and a destination (D), where RIS is used as a transmitter along with the RF signal generator, as shown in Figure 2. In addition, we assume that the RIS and RF signal generators act together as a transmitter as in [59]. Thus, the signal at D is given as follows.

$$y_D = (\beta_D \beta_S + \bar{\beta}_D \bar{\beta}_S^*) \sqrt{\frac{P_S}{d_2^\chi}} \sum_{n=1}^N h_{D,n} e^{j\phi_n} x + (\beta_D \bar{\beta}_S + \bar{\beta}_D \beta_S^*) \sqrt{\frac{P_S}{d_2^\chi}} \sum_{n=1}^N h_{D,n} e^{j\phi_n} x^* + \beta_D n_0 + \bar{\beta}_D n_0^* \tag{6}$$

Based on [59], the maximum SNR at user D is given as follows:

$$\gamma_D = \frac{P_S \left[\sum_{n=1}^N A_n \right]^2 \omega_1}{P_S \left[\sum_{n=1}^N A_n \right]^2 \omega_2 + d_2^\chi N_0 \omega_3} = \frac{\bar{\eta} \omega_1}{\bar{\eta} \omega_2 + \omega_3} \tag{7}$$

where A_n is a Rayleigh random variable with mean $\sqrt{\pi}/2$ and variance $\frac{(4-\pi)}{4}$ and $\bar{\eta} = \frac{\rho_S}{d_2^\chi} X^2$.

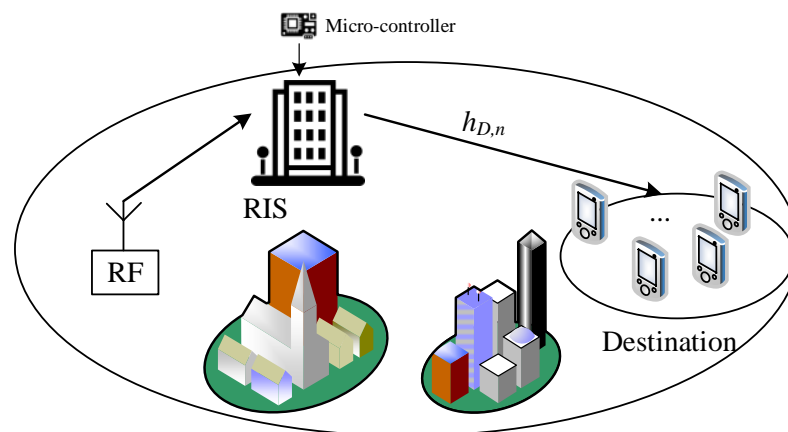


Figure 2. System model for RIS acting as a transmitter.

3. Performance Analysis

In this section, we analyze the outage probability and ergodic capacity for the RIS-DH case and the RIS-T case in the presence of IQI. To provide more insight into the RIS-aided scheme, an asymptotic analysis is presented, and a benchmark scheme is also mentioned in Figure 3.

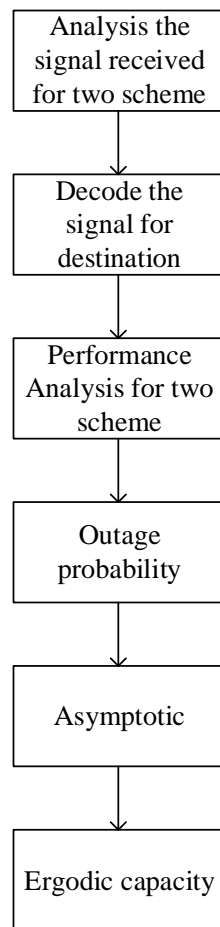


Figure 3. The flowchart to calculate the main system metrics for the RIS-T scheme.

3.1. Outage Probability for RIS-DH Scheme

The outage probability of the system is written as follows:

$$P_{DH,out} = \Pr(\gamma_D < \gamma_{th}), \tag{8}$$

where γ_{th} denotes the target rate. With the help of (5), we can rewrite (8) as follows.

$$\begin{aligned} P_{DH,out} &= \Pr\left(\eta < \frac{\gamma_{th}\omega_3}{\omega_1 - \gamma_{th}\omega_2}\right) \\ &= F_\eta\left(\frac{\gamma_{th}\omega_3}{\omega_1 - \gamma_{th}\omega_2}\right). \end{aligned} \tag{9}$$

3.1.1. NCCS Distribution

As reported in [58], the probability density function (PDF) of Z^2 is given as follows:

$$f_{Z^2}(x) = \frac{1}{2\sigma^2} \left(\frac{x}{\lambda}\right)^{-\frac{1}{4}} e^{-\frac{x+\lambda}{2\sigma^2}} I_{-\frac{1}{2}}\left(\frac{\sqrt{x\lambda}}{\sigma^2}\right), \tag{10}$$

where $\lambda = (\frac{N\pi}{4})^2$, $\sigma^2 = N(1 - \frac{\pi^2}{16})^2$ and $I_v(\bullet)$ denotes the Bessel functions of the first class with order v [60]. Moreover, the PDF of η can be expressed as follows.

$$f_{\eta}(x) = \frac{e^{-\frac{\lambda}{2\sigma^2}}}{2\sigma^2 \left(\frac{\rho_S}{d_1^{\chi} d_2^{\chi}}\right)^{\frac{3}{4}}} \left(\frac{x}{\lambda}\right)^{-\frac{1}{4}} \times e^{-\frac{d_1^{\chi} d_2^{\chi} x}{2\rho_S \sigma^2}} I_{-\frac{1}{2}} \left(\frac{\sqrt{d_1^{\chi} d_2^{\chi} x \lambda}}{\sqrt{\rho_S \sigma^2}}\right). \tag{11}$$

Based on ([60], Eq. 8.445), the cumulative distribution function (CDF) of η is written as follows:

$$F_{\eta}(x) = 1 - Q_{\frac{1}{2}} \left(\frac{\sqrt{\lambda}}{\sigma}, \sqrt{\frac{d_1^{\chi} d_2^{\chi} x}{\rho_S \sigma^2}}\right) = \sum_{k=0}^{\infty} \frac{e^{-\frac{\lambda}{2\sigma^2}}}{k! \Gamma(k + \frac{1}{2})} \left(\frac{\lambda}{2\sigma^2}\right)^k \gamma\left(k + \frac{1}{2}, \frac{d_1^{\chi} d_2^{\chi} x}{2\rho_S \sigma^2}\right). \tag{12}$$

where $Q_m(a; b)$ is the Marcum Q-function [61] and $\gamma(\bullet, \bullet)$ is gamma incomplete [60].

Based on the CDF in (12), the closed-form of P_{out} can be expressed as follows.

$$P_{DH,out} = \sum_{k=0}^{\infty} \frac{e^{-\frac{\lambda}{2\sigma^2}}}{k! \Gamma(k + \frac{1}{2})} \left(\frac{\lambda}{2\sigma^2}\right)^k \times \gamma\left(k + \frac{1}{2}, \frac{\gamma_{th} \omega_3 d_1^{\chi} d_2^{\chi}}{2\sigma^2 \rho_S (\omega_1 - \gamma_{th} \omega_2)}\right). \tag{13}$$

3.1.2. K_g Distribution

In this section, we present the analysis by using the K_G distribution as in [62]. Next, the PDF of Z is given as follows [62]:

$$f_Z(x) = \frac{4\Psi^{k+m} x^{k+m-1}}{\Gamma(k)\Gamma(m)} K_{k-m}(2\Psi x). \tag{14}$$

where $k = \frac{-b + \sqrt{b^2 - 4ac}}{2a}$ and $m = \frac{-b - \sqrt{b^2 - 4ac}}{2a}$ are the shaping parameters, $\Gamma(\cdot)$ is the gamma function [63], $K_x(\cdot)$ is the modified Bessel function of the second kind with zero order [60], $\Psi = \sqrt{\frac{km}{\Omega}}$, and $\Omega = \mu_Z(2)$ is the mean power. Moreover, the parameters a , b , and c have been defined previously [63]. Their values are related to moment $\mu_Z(\cdot)$ of R , which is defined as follows:

$$\mu_Z(n) = \sum_{n_1=0}^n \sum_{n_2=0}^{n_1} \dots \sum_{n_{N-1}=0}^{n_{N-2}} \binom{n}{n_1} \binom{n_1}{n_2} \dots \binom{n_{N-2}}{n_{N-1}} \times \mu_{\chi^i}(n - n_1) \mu_{\chi^2}(n_1 - n_2) \dots \mu_{\chi^{N-1}}(n_{N-1}), \tag{15}$$

where $\mu_{\chi^i}(n) = \Gamma^2(1 + \frac{n}{2})$ is the n th moment of χ^i . In addition, k and m are real numbers. When k and m are conjugate complex numbers, k and m are set to the estimated modulus values of the conjugate complex number.

Based on (9), we can express the PDF of η as follows.

$$f_{\eta}(x) = \frac{2\Psi^{k+m} x^{\frac{k+m}{2}-1}}{\Gamma(k)\Gamma(m) \left(\frac{\rho_S}{d_1^{\lambda} d_2^{\lambda}}\right)^{\frac{k+m}{2}}} K_{k-m} \left(2\Psi \sqrt{\frac{d_1^{\lambda} d_2^{\lambda} x}{\rho_S}} \right). \tag{16}$$

Then, the CDF can be obtained as follows.

$$F_{\eta}(x) = \frac{1}{\Gamma(k)\Gamma(m)} G_{1,3}^{2,1} \left[\frac{d_1^{\lambda} d_2^{\lambda} \Psi^2}{\rho_S} x \mid \begin{matrix} 1 \\ k, m, 0 \end{matrix} \right]. \tag{17}$$

For the K_G case, the closed-form of P_{out} is given as follows.

$$P_{DH,out} = \frac{1}{\Gamma(k)\Gamma(m)} G_{1,3}^{2,1} \left[\frac{d_1^{\lambda} d_2^{\lambda} \gamma_{th} \omega_3 \Psi^2}{\rho_S (\omega_1 - \gamma_{th} \omega_2)} \mid \begin{matrix} 1 \\ k, m, 0 \end{matrix} \right]. \tag{18}$$

Remark 1. The outage performance of the two schemes mostly depends on transmit SNR at the access point ρ_S , shown in (18). Furthermore, the impact of IQI can be observed in (9). The performance gaps of practical scenarios will be analyzed to provide guidelines for RIS deployment in suitable applications in IoT systems. Therefore, we expect that the improved performance at destination users could be adjusted by main parameters such as ρ_S and the configuration of RIS as well.

3.2. Asymptotic Analysis for RIS-DH Scheme

In this section, we analyze the asymptotic when $\rho_S \rightarrow \infty$.

3.2.1. NCCS Distribution

Based on ([60], Eq. 8.354.1), we have the following.

$$\gamma(a, x) \xrightarrow{x \rightarrow \infty} \frac{x^a}{a} \tag{19}$$

In this case, substituting (19) into (13), we have the asymptotic of $P_{DH,out}^{\infty}$ as follows.

$$P_{DH,out}^{\infty} = \sum_{k=0}^{\infty} \frac{e^{-\frac{\lambda}{2\sigma^2}}}{k! \Gamma(k + \frac{3}{2})} \left(\frac{\lambda}{2\sigma^2}\right)^k \times \left(\frac{d_1^{\lambda} d_2^{\lambda} \gamma_{th} \omega_3}{2\sigma^2 \rho_S (\omega_1 - \gamma_{th} \omega_2)}\right)^{k+\frac{1}{2}} \tag{20}$$

3.2.2. K_g Distribution

As [64], we can write the asymptotic PDF for (11) as follows.

$$f_{\eta}(x) \approx \frac{2\Psi^{k+m}}{\Gamma(k)\Gamma(m) \left(\frac{\rho_S}{d_1^{\lambda} d_2^{\lambda}}\right)^{\frac{k+m}{2}}} x^{\frac{k+m}{2}-1}. \tag{21}$$

Then, we can obtain the asymptotic of $P_{DH,out}^{\infty}$ as follows.

$$P_{DH,out}^{\infty} \approx \frac{4\Psi^{k+m}}{\Gamma(k)\Gamma(m)(k+m)} \left(\frac{d_1^{\lambda} d_2^{\lambda} \gamma_{th} \omega_3}{\rho_S (\omega_1 - \gamma_{th} \omega_2)}\right)^{\frac{k+m}{2}}. \tag{22}$$

3.3. Outage Probability for RIS-T Scheme

Similarly [63], the PDF of X^2 is given as follows:

$$f_{X^2}(x) \approx \frac{x^{N-1}e^{-\frac{x}{B}}}{B^N(N-1)!} \tag{23}$$

where $B = 1 + (N - 1)\Gamma^2(\frac{3}{2})$. Then, following the result in ([60], Eq. 3.351.1), the CDF of X^2 is obtained as follows.

$$F_{X^2}(x) = \frac{\gamma(N, \frac{x}{B})}{\Gamma(N)}. \tag{24}$$

With the help of (7), the outage probability of RIS-T scheme is given as follows.

$$P_{T,out} = \frac{\gamma\left(N, \frac{d_2^X \gamma_{th} \omega_3}{B \rho_S (\omega_1 - \gamma_{th} \omega_2)}\right)}{\Gamma(N)}. \tag{25}$$

3.4. Asymptotic Analysis for RIS-T Scheme

Taking advantage of the result in (19), the asymptotic of P^∞ is expressed as follows.

$$P_{T,out}^\infty \approx \frac{1}{\Gamma(N+1)} \left(\frac{d_2^X \gamma_{th} \omega_3}{B \rho_S (\omega_1 - \gamma_{th} \omega_2)} \right)^N. \tag{26}$$

4. Ergodic Capacity Analysis

The outage probability is the first step to consider how the system works at the destination. It is suitable to examine the delay-limited transmission mode, but to evaluate performance for delay-tolerant transmission mode, ergodic capacity is a further metric that has to be calculated in closed-form. The ergodic capacity can be calculated as follows.

$$\begin{aligned} C &= E[\log_2(1 + \gamma_D)] \\ &= \frac{1}{\ln(2)} \int_0^{\frac{\omega_1}{\omega_2}} \frac{1 - F_{\gamma_D}(x)}{1 + x} dx. \end{aligned} \tag{27}$$

4.1. RIS-DH Case

4.1.1. NCCS Distribution

With the help of (8), we can write the following.

$$\begin{aligned} C_{DH} &= \frac{1}{\ln(2)} \sum_{k=0}^{\infty} \frac{e^{-\frac{\lambda}{2\sigma^2}}}{k! \Gamma(k + \frac{1}{2})} \left(\frac{\lambda}{2\sigma^2} \right)^k \\ &\times \int_0^{\frac{\omega_1}{\omega_2}} \frac{\Gamma\left(k + \frac{1}{2}, \frac{d_1^X d_2^X x \omega_3}{2\sigma^2 \rho_S (\omega_1 - x \omega_2)}\right)}{1 + x} dx. \end{aligned} \tag{28}$$

By using the Gaussian–Chebyshev Quad with $\delta_k = \cos\left(\frac{2k-1}{2I}\pi\right)$, we can make the following approximation.

$$C_{DH} \approx \frac{\omega_1\pi}{I \ln(2)} \sum_{k=0}^{\infty} \frac{e^{-\frac{\lambda}{2\sigma^2}}}{k! \Gamma\left(k + \frac{1}{2}\right)} \left(\frac{\lambda}{2\sigma^2}\right)^k \times \sum_{k=1}^I \sqrt{1 - \delta_k^2} \frac{\Gamma\left(k + \frac{1}{2}, \frac{d_1^\chi d_2^\chi \omega_3 (1 + \delta_k)}{2\sigma^2 \rho_S \omega_2 (1 - \delta_k)}\right)}{2\omega_2 + \omega_1 (1 + \delta_k)}. \tag{29}$$

4.1.2. K_g Distribution

Substituting (17) and after some computations, we have the following.

$$C_{DH} = \frac{1}{\ln(2)\Gamma(k)\Gamma(m)} \times \int_0^{\frac{\omega_1}{\omega_2}} G_{1,3}^{3,0} \left[\frac{x d_1^\chi d_2^\chi \omega_3 \Psi^2}{(\omega_1 - x \omega_2) \rho_S} \middle| \begin{matrix} 1 \\ k, m, 0 \end{matrix} \right] \frac{1}{1+x} dx. \tag{30}$$

Similarly, the closed-form of C can be approximated as follows.

$$C_{DH} \approx \frac{\omega_1\pi}{I \ln(2)\Gamma(k)\Gamma(m)(2\omega_2 + \omega_1(1 + \delta_k))} \times \sum_{k=1}^I \sqrt{1 - \delta_k^2} G_{1,3}^{3,0} \left[\frac{d_1^\chi d_2^\chi \omega_3 \Psi^2 (1 + \delta_k)}{2\omega_2 \rho_S (1 - \delta_k)} \middle| \begin{matrix} 1 \\ k, m, 0 \end{matrix} \right]. \tag{31}$$

4.2. RIS-T Case

The ergodic capacity in RIS-T case is calculated as follows.

$$C_T = \frac{1}{\ln(2)\Gamma(N)} \int_0^{\frac{\omega_1}{\omega_2}} \Gamma\left(N, \frac{x d_2^\chi \omega_3}{B \rho_S (\omega_1 - x \omega_2)}\right) \frac{1}{1+x} dx. \tag{32}$$

Finally, the closed-form ergodic capacity in RIS-T case can be obtained as follows.

$$C_T \approx \frac{\pi}{I \ln(2)\Gamma(N)} \sum_{k=1}^I \sqrt{1 - \delta_k^2} \frac{\omega_1 \Gamma\left(N, \frac{(1 + \delta_k) d_2^\chi \omega_3}{B \rho_S \omega_2 (1 - \delta_k)}\right)}{2\omega_2 + (1 + \delta_k) \omega_1}. \tag{33}$$

Since ergodic capacity is the second metric, we expect that some parameters can be adjusted at the RIS and the source to deal with the worse situation at the destination. For example, when the destination is located a far distance from the source, it is predicted that the phase factor of RIS elements and the number of RIS element will contribute to the system improvement.

5. Numerical Results and Discussions

In this section, we present and discuss some results from the mathematical expressions derived in the paper. We set $\chi = 2$, $\gamma_{th} = 5$ dB, $\mu_T = \mu_R = 1.05$, $v_T = v_R = 25^\circ$, $d_1 = 5$ m, and $d_2 = 5$ m.

In Figure 4, we depict outage performance of RIS-aided system, which benefits from dual-hop transmission. When ρ_S increases, SNR can be enhanced, then outage performance can be improved as well. In this RIS-DH scheme, a higher number of meta-surface N leads to significant improvement in terms of outage probability. It can be observed that the

simulated curves match very tightly with the analytical curves, which confirms the validity of derived expressions. We also compare the outage performance between the NCCS and the K_G distributions, which shows that the K_G distribution exhibits better performance. Under the impact of IQI, we can see a slight reduction in outage probability for such an RIS-DH scheme. It is a valid result when we see clearly that asymptotic lines are matched with exact curves at high SNR at the source. It means that IQI reduces the system performance. However, at high SNR regime, system performance still looks good enough to guarantee that such forms of transmission better serve mobile users.

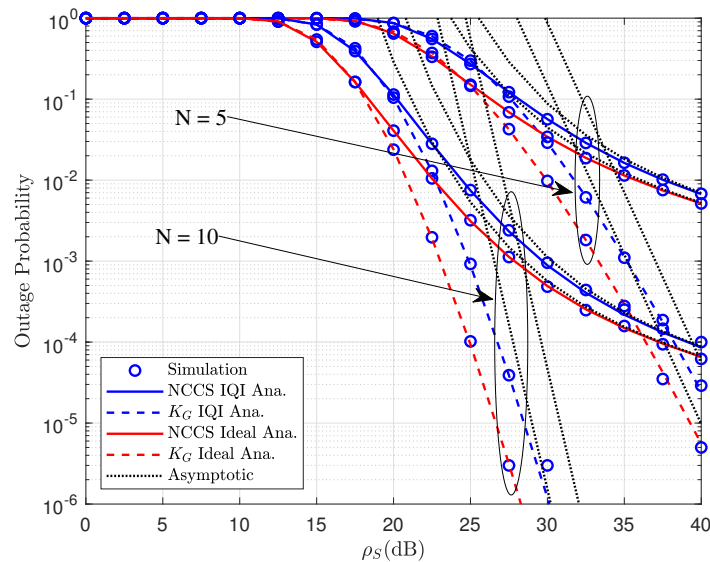


Figure 4. The outage probability vs. ρ_S (dB) with varying N for RIS-DH case.

In Figure 5, we illustrate the curves for the outage probability for the RIS-T case. We consider two cases: $N = 2$ and $N = 5$. By varying the number of meta-surface N , a big gap emerges, which confirms the important role of RIS to achieve improvements in such an RIS-T scheme. It is a very valuable result since we observed that the analytical results are highly consistent with the Monte-Carlo based simulation.

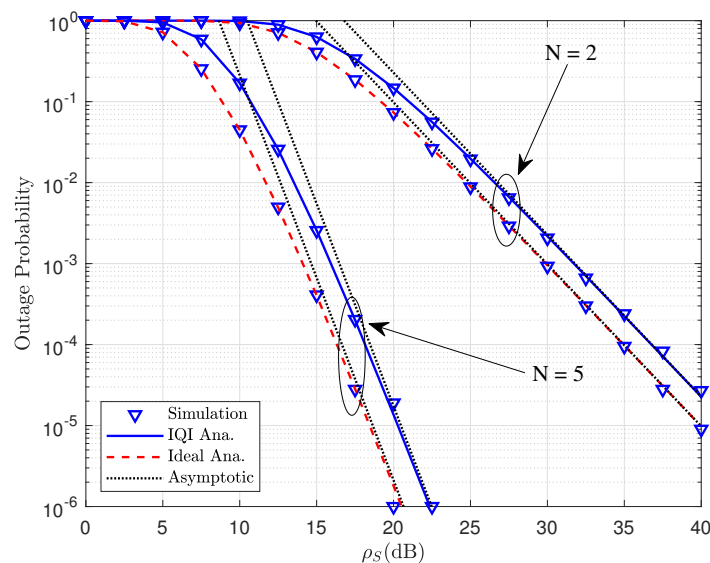


Figure 5. The outage probability vs. ρ_S (dB) with varying N for RIS-T case.

As observed in Figure 6, the SNR threshold γ_{th} has the main role to limit performance as expected. In this case, the simulation results are also consistent with the analytical

results. Similar observations can be seen in Figure 7. Although higher SNRs at source ρ_S contribute to increasing outage performance, it depends on other parameters. From the results reported in Figure 7, one can observe that the slope of the NCCS distribution curves approach saturation regardless of the value of ρ_S . The threshold rate holds crucial impact on the system performance. Therefore, depending on the demand of service at users, the system should balance the quality targeted to each user regardless of the impact of IQI.

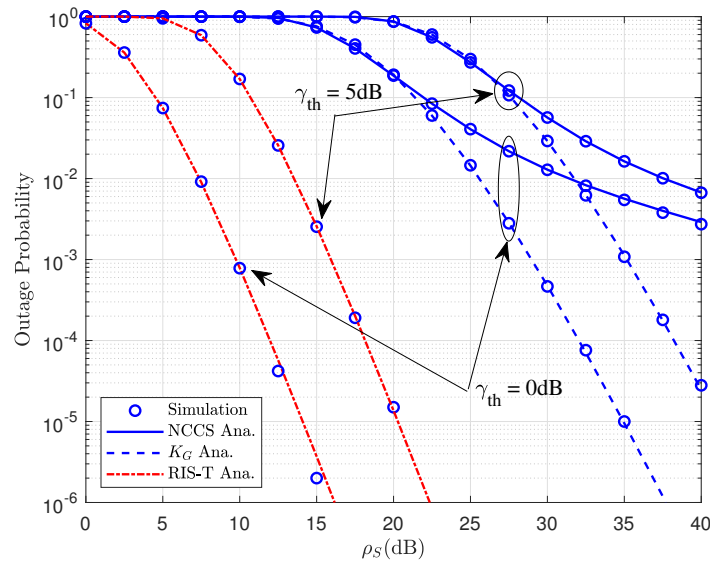


Figure 6. The outage probability vs. ρ_S (dB) with varying γ_{th} .

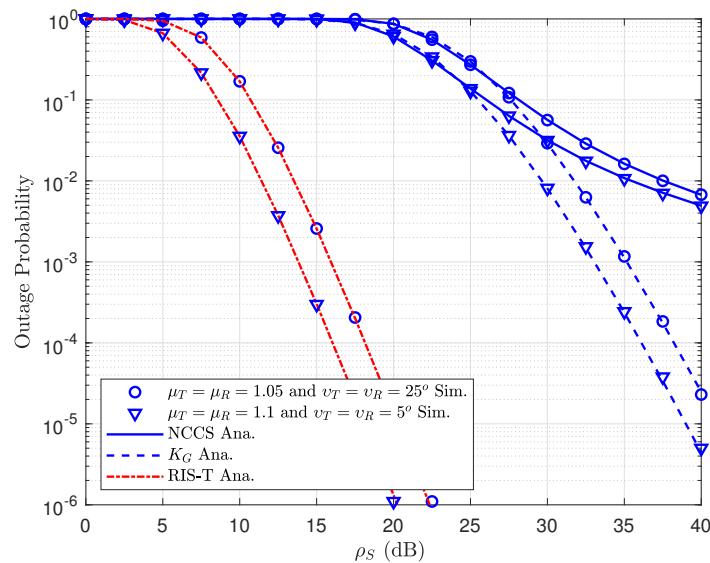


Figure 7. The outage probability vs. ρ_S (dB) with varying $\mu_T = \mu_R$ and $v_T = v_R$ with $N = 5$.

Next, Figure 8 is conceived for the RIS-DH case, we show the ergodic capacity performance versus transmit SNR at the access point. We can see that ergodic capacity can be improved once transmit SNR is higher at the access point. This can be explained by the fact that the formulation of ergodic rate in all scenarios of channel distributions depends on SNR at the destination, which relies on SNR at the source. However, at high SNR regime, the ergodic capacity shows its saturation threshold except for the K_G channel distribution and ideal IQI. It can be observed that it becomes prominent when considering gaps between K_G channel distribution of ideal IQI and other cases when transmit SNR at the access point is greater than 25. This trend of the figure confirms the crucial impact of IQI on the ergodic capacity that occurs at high SNR regimes.

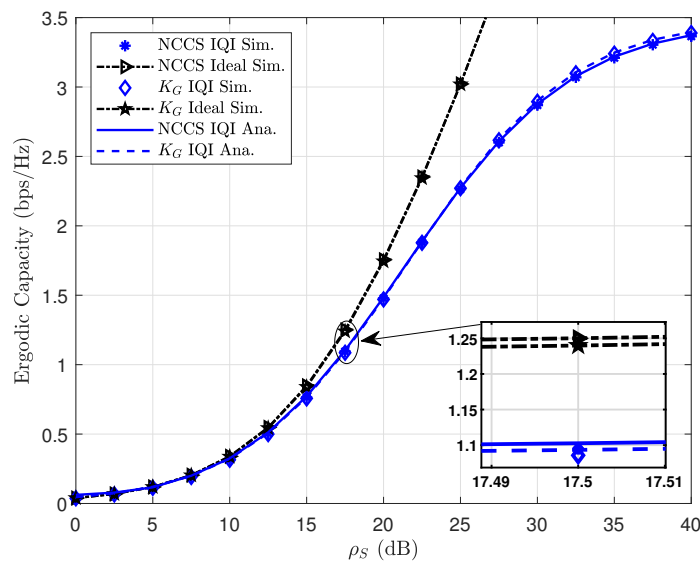


Figure 8. The ergodic capacity vs. ρ_S (dB) for RIS-DH case with $N = 2$.

Similar observations can be achieved in the RIS-T case, as shown in Figure 9. We show the ergodic capacity of the considered system corresponding to two values of meta-surface, i.e., $N = 2$ and $N = 5$. The most significant difference is a gap between ideal and IQI systems occurring in a entire range of transmit SNR. If we focus on the specific point of SNR 10 dB, the influence of IQI is too significant, and it leads to saturation lines for ergodic capacity regardless of the modification of the number of meta-surface in RIS.

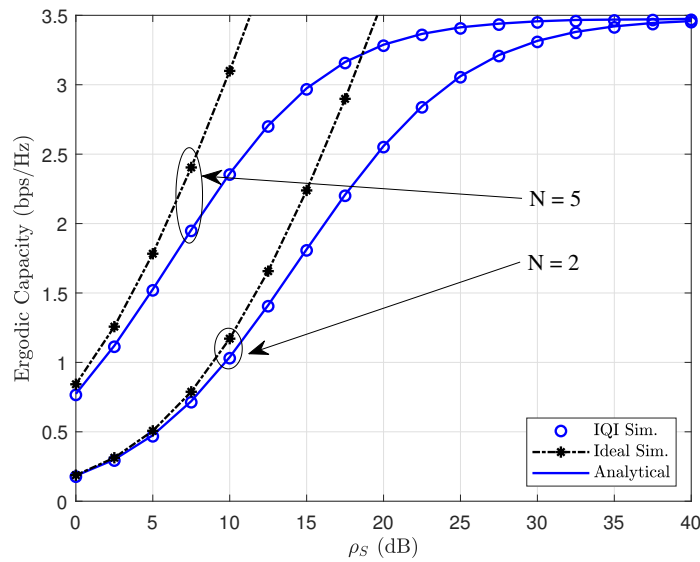


Figure 9. The ergodic capacity vs. ρ_S (dB) for RIS-T case.

In Figure 10, we can observe the impact on ergodic capacity when varying $\mu_T = \mu_R$ and $v_T = v_R$ with $N = 2$. We can see that with $\mu_T = \mu_R = 1.05$ and $v_T = v_R = 25^\circ$, the RIS-T and NCCS curves approach a ceiling at high SNR. Although SNR at the source can be increased; however, the ergodic capacity stills has an upper limit. It is worth noting that the proposed system can work well once some parameters are controlled well, such as the transmit SNR, levels of IQI, and structure of RIS components.

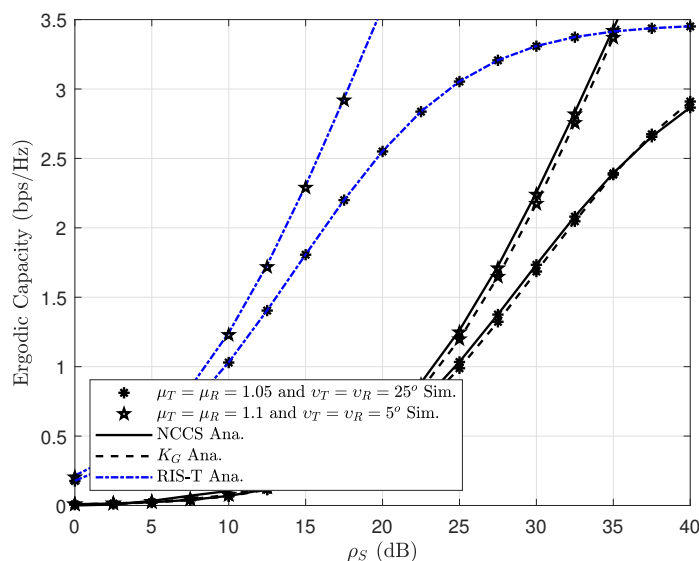


Figure 10. The outage probability vs. ρ_S (dB) with varying $\mu_T = \mu_R$ and $v_T = v_R$ with $N = 2$.

6. Conclusions

We have evaluated the system performance of the RIS-aided system by exploring NCCS and K_G distributions of channels. We compared system performance under the impact of IQI and the number of meta-surface N of a RIS. More importantly, we derived expressions of outage probability and ergodic capacity in closed-form. Simulation results showed that the significant improvement of outage probability can be obtained at high SNR and high meta-surface N . Moreover, there should be a limited impact of IQI levels on such a system. Furthermore, both schemes can provide guidelines to employ the RIS system under the impact of IQI. Finally, in terms of ergodic capacity, although SNR at the source can be increased, the ergodic capacity faces an upper limit. Despite this limitation, the proposed system can work well once some parameters are controlled well, such as the transmit SNR, levels of IQI, and the number of RIS components. As a potential future work, other distributions of channel should be examined; for example, Rician fading can be taken into account, and more system metrics can also be explored.

Author Contributions: N.D.N. introduced the idea, contributed to developing some mathematical analysis; A.-T.L. performed the simulation experiments; M.M. contributed to prepare manuscript; F.A. and E.P. provided valuable comments. All authors have read and agreed to the published version of the manuscript.

Funding: This research was partly supported by Van Lang University under Project 1000.

Acknowledgments: This work has been partly supported by Van Lang University under Project 1000.

Conflicts of Interest: The authors declare no conflict of interest.

References

1. Liu, Y.; Liu, E.; Wang, R.; Geng, Y. Channel Estimation and Power Scaling of Reconfigurable Intelligent Surface with Non-Ideal Hardware. In Proceedings of the 2021 IEEE Wireless Communications and Networking Conference (WCNC), Nanjing, China, 29 March–1 April 2021.
2. Hemanth, A.; Umamaheswari, K.; Pogaku, A.C.; Do, D.-T.; Lee, B.M. Outage Performance Analysis of Reconfigurable Intelligent Surfaces-Aided NOMA under Presence of Hardware Impairment. *IEEE Access* **2020**, *8*, 212156–212165. [\[CrossRef\]](#)
3. Gong, S.; Lu, X.; Hoang, D.T.; Niyato, D.; Shu, L.; Kim, D.I.; Liang, Y.C. Towards smart radio environment for wireless communications via intelligent reflecting surfaces: A comprehensive survey. *IEEE Commun. Surv. Tutor.* **2020**, *22*, 2283–2314. [\[CrossRef\]](#)
4. Nguyen, M.-S.V.; Do, Di.; Al-Rubaye, S.; Mumtaz, S.; Al-Dulaimi, A.; Dobre, O. Exploiting Impacts of Antenna Selection and Energy Harvesting for Massive Network Connectivity. *IEEE Trans. Commun.* **2021**, *69*, 7587–7602. [\[CrossRef\]](#)
5. Do, Di.; Le, An.; Liu, Y.; Jamalipour, A. User Grouping and Energy Harvesting in UAV-NOMA System with AF/DF Relaying. *IEEE Trans. Veh. Technol.* **2021**, *70*, 11855–11868. [\[CrossRef\]](#)

6. Wu, Q.; Zhang, R. Towards smart and reconfigurable environment: Intelligent reflecting surface aided wireless network. *IEEE Commun. Mag.* **2020**, *58*, 106–112. [\[CrossRef\]](#)
7. Yan, W.; Yuan, X.; He, Z.-Q.; Kuai, X. Passive beamforming and information transfer design for reconfigurable intelligent surfaces aided multiuser MIMO systems. *IEEE J. Sel. Areas Commun.* **2020**, *38*, 1793–1808. [\[CrossRef\]](#)
8. Yang, G.; Liang, Y.; Zhang, R.; Pei, Y. Modulation in the air: Backscatter communication over ambient OFDM carrier. *IEEE Trans. Commun.* **2018**, *66*, 1219–1233. [\[CrossRef\]](#)
9. Guo, S.; Lv, S.; Zhang, H.; Ye, J.; Zhang, P. Reflecting modulation. *IEEE J. Sel. Areas Commun.* **2020**, *38*, 2548–2561. [\[CrossRef\]](#)
10. Pan, C.; Ren, H.; Wang, K.; Xu, W.; Elkashlan, M.; Nallanathan, A.; Hanzo, L. Multicell MIMO communications relying on intelligent reflecting surfaces. *IEEE Trans. Wirel. Commun.* **2020**, *19*, 5218–5233. [\[CrossRef\]](#)
11. Xie, H.; Xu, J.; Liu, Y. Max-Min Fairness in IRS-Aided Multi-Cell MISO Systems via Joint Transmit and Reflective Beamforming. In Proceedings of the ICC 2020—2020 IEEE International Conference on Communications (ICC), Dublin, Ireland, 7–11 June 2020; pp. 1–6
12. Hu, S.; Wei, Z.; Cai, Y.; Ng, D.W.K.; Yuan, J. Sum-Rate Maximization for Multiuser MISO Downlink Systems with Self-Sustainable IRS. *arXiv* **2020**, arXiv:2005.11663.
13. Hua, M.; Wu, Q.; Ng, D.W.K.; Zhao, J.; Yang, L. Intelligent reflecting surface-aided joint processing coordinated multi-point transmission. *arXiv* **2020**, arXiv:2003.13909.
14. Wu, Q.; Zhang, R. Joint active and passive beamforming optimization for intelligent reflecting surface assisted SWIPT under QoS constraints. *IEEE J. Sel. Areas Commun.* **2020**, *38*, 1735–1748. [\[CrossRef\]](#)
15. Wu, Q.; Zhang, R. Weighted sum power maximization for intelligent reflecting surface aided SWIPT. *IEEE Wirel. Commun. Lett.* **2020**, *9*, 586–590. [\[CrossRef\]](#)
16. Hua, M.; Yang, L.; Wu, Q.; Pan, C.; Li, C.; Swindlehurst, A.L. UAV-Assisted Intelligent Reflecting Surface Symbiotic Radio System. *IEEE Trans. Wirel. Commun.* **2021**, *20*, 5769–5785. [\[CrossRef\]](#)
17. Le, A.-T.; Ha, N.-D.X.; Do, Di.; Silva, A.; Yadav, S. Enabling User Grouping and Fixed Power Allocation Scheme for Reconfigurable Intelligent Surfaces-Aided Wireless Systems. *IEEE Access* **2021**, *9*, 92263–92275. [\[CrossRef\]](#)
18. Le, C.-B.; Do, D.-T.; Li, X.; Huang, Y.-F.; Chen, H.-C.; Voznak, M. Enabling NOMA in Backscatter Reconfigurable Intelligent Surfaces-Aided Systems. *IEEE Access* **2021**, *9*, 33782–33795. [\[CrossRef\]](#)
19. Guan, X.; Wu, Q.; Zhang, R. Intelligent reflecting surface assisted secrecy communication: Is artificial noise helpful or not? *IEEE Wirel. Commun. Lett.* **2020**, *9*, 778–782. [\[CrossRef\]](#)
20. Shen, H.; Xu, W.; Gong, S.; He, Z.; Zhao, C. Secrecy rate maximization for intelligent reflecting surface assisted multi-antenna communications. *IEEE Commun. Lett.* **2019**, *23*, 1488–1492. [\[CrossRef\]](#)
21. Guan, X.; Wu, Q.; Zhang, R. Joint power control and passive beamforming in IRS-assisted spectrum sharing. *IEEE Commun. Lett.* **2020**, *24*, 1153–1157. [\[CrossRef\]](#)
22. Bai, T.; Pan, C.; Deng, Y.; Elkashlan, M.; Nallanathan, A.; Hanzo, L. Latency minimization for intelligent reflecting surface aided mobile edge computing. *IEEE J. Sel. Areas Commun.* **2020**, *38*, 2666–2682. [\[CrossRef\]](#)
23. Nadeem, Q.-U.-A.; Kammoun, A.; Chaaban, A.; Debbah, M.; Alouini, M.-S. Asymptotic max-min SINR analysis of reconfigurable intelligent surface assisted MISO systems. *IEEE Trans. Wirel. Commun.* **2020**, *19*, 7748–7764. [\[CrossRef\]](#)
24. Zhao, M.-M.; Wu, Q.; Zhao, M.-J.; Zhang, R. Intelligent reflecting surface enhanced wireless network: Two-timescale beamforming optimization. *arXiv* **2020**, arXiv:1912.01818.
25. Zhao, M.-M.; Wu, Q.; Zhao, M.-J.; Zhang, R. Exploiting amplitude control in intelligent reflecting surface aided wireless communication with imperfect CSI. *arXiv* **2020**, arXiv:2005.07002.
26. Zhou, G.; Pan, C.; Ren, H.; Wang, K.; Nallanathan, A. A framework of robust transmission design for IRS-aided MISO communications with imperfect cascaded channels. *IEEE Trans. Signal Process.* **2020**, *68*, 5092–5106. [\[CrossRef\]](#)
27. Zhou, G.; Pan, C.; Ren, H.; Wang, K.; Renzo, M.D.; Nallanathan, A. Robust beamforming design for intelligent reflecting surface aided MISO communication systems. *IEEE Wirel. Commun. Lett.* **2020**, *9*, 1658–1662. [\[CrossRef\]](#)
28. Hu, C.; Dai, L. Two-timescale channel estimation for reconfigurable intelligent surface aided wireless communications. *arXiv* **2020**, arXiv:1912.07990.
29. Wang, Z.; Liu, L.; Cui, S. Channel estimation for intelligent reflecting surface assisted multiuser communications: Framework, algorithms, and analysis. *IEEE Trans. Wirel. Commun.* **2020**, *19*, 6607–6620. [\[CrossRef\]](#)
30. Chen, J.; Liang, Y.-C.; Cheng, H.V.; Yu, W. Channel estimation for reconfigurable intelligent surface aided multi-user MIMO systems. *arXiv* **2019**, arXiv:1912.03619.
31. Trigui, I.; Agbogla, E.K.; Benjillali, M.; Ajib, W.; Zhu, W.-P. Bit Error Rate Analysis for Reconfigurable Intelligent Surfaces with Phase Errors. *IEEE Commun. Lett.* **2021**, *25*, 2176–2180. [\[CrossRef\]](#)
32. Mao, Z.; Peng, M.; Liu, X. Channel estimation for reconfigurable intelligent surface assisted wireless communication systems in mobility scenarios. *China Commun.* **2021**, *18*, 29–38. [\[CrossRef\]](#)
33. Sun, S.; Yan, H. Channel Estimation for Reconfigurable Intelligent Surface-Assisted Wireless Communications Considering Doppler Effect. *IEEE Wirel. Commun. Lett.* **2021**, *10*, 790–794. [\[CrossRef\]](#)
34. Li, L.; Ma, D.; Ren, H.; Wang, D.; Tang, X.; Liang, W.; Bai, T. Enhanced reconfigurable intelligent surface assisted mmWave communication: A federated learning approach. *China Commun.* **2020**, *17*, 115–128. [\[CrossRef\]](#)

35. Jin, Y.; Zhang, J.; Zhang, X.; Xiao, H.; Ai, B.; Ng, D.W.K. Channel Estimation for Semi-Passive Reconfigurable Intelligent Surfaces With Enhanced Deep Residual Networks. *IEEE Trans. Veh. Technol.* **2021**, *70*, 11083–11088. [[CrossRef](#)]
36. Jin, Y.; Zhang, J.; Huang, C.; Yang, L.; Xiao, H.; Ai, B.; Wang, Z. Multiple Residual Dense Networks for Reconfigurable Intelligent Surfaces Cascaded Channel Estimation. *IEEE Trans. Veh. Technol.* **2021**, *71*, 2134–2139. [[CrossRef](#)]
37. Zhang, S.; Li, M.; Jian, M.; Zhao, Y.; Gao, F. AIRIS: Artificial intelligence enhanced signal processing in reconfigurable intelligent surface communications. *China Commun.* **2021**, *18*, 158–171. [[CrossRef](#)]
38. Sheen, B.; Yang, J.; Feng, X.; Chowdhury, M.M.U. A Deep Learning Based Modeling of Reconfigurable Intelligent Surface Assisted Wireless Communications for Phase Shift Configuration. *IEEE Open J. Commun. Soc.* **2021**, *2*, 262–272. [[CrossRef](#)]
39. Zhou, Z.; Ge, N.; Wang, Z.; Hanzo, L. Joint Transmit Precoding and Reconfigurable Intelligent Surface Phase Adjustment: A Decomposition-Aided Channel Estimation Approach. *IEEE Trans. Commun.* **2021**, *69*, 1228–1243. [[CrossRef](#)]
40. Zhi, K.; Pan, C.; Ren, H.; Wang, K. Statistical CSI-Based Design for Reconfigurable Intelligent Surface-Aided Massive MIMO Systems with Direct Links. *IEEE Wirel. Commun. Lett.* **2021**, *10*, 1128–1132. [[CrossRef](#)]
41. Shi, Z.; Wang, H.; Fu, Y.; Yang, G.; Ma, S.; Gao, F. Outage Analysis of Reconfigurable Intelligent Surface Aided MIMO Communications with Statistical CSI. *IEEE Trans. Wirel. Commun.* **2021**, *21*, 823–839. [[CrossRef](#)]
42. Liu, H.; Yuan, X.; Zhang, Y.-J.A. Matrix-Calibration-Based Cascaded Channel Estimation for Reconfigurable Intelligent Surface Assisted Multiuser MIMO. *IEEE J. Sel. Areas Commun.* **2020**, *38*, 2621–2636. [[CrossRef](#)]
43. Wu, Q.; Zhang, R. Intelligent reflecting surface enhanced wireless network via joint active and passive beamforming. *IEEE Trans. Wirel. Commun.* **2019**, *18*, 5394–5409. [[CrossRef](#)]
44. Pan, C.; Ren, H.; Wang, K.; Elkashlan, M.; Nallanathan, A.; Wang, J.; Hanzo, L. Intelligent reflecting surface aided MIMO broadcasting for simultaneous wireless information and power transfer. *arXiv* **2020**, arxiv:1908.04863.
45. Du, H.; Zhang, J.; Cheng, J.; Ai, B. Millimeter Wave Communications with Reconfigurable Intelligent Surfaces: Performance Analysis and Optimization. *IEEE Trans. Commun.* **2021**, *69*, 2752–2768. [[CrossRef](#)]
46. Xu, J.; Ai, B. When mmWave High-Speed Railway Networks Meet Reconfigurable Intelligent Surface: A Deep Reinforcement Learning Method. *IEEE Wirel. Commun. Lett.* **2021**, *11*, 533–537. [[CrossRef](#)]
47. Liu, H.; Zhang, J.; Wu, Q.; Xiao, H.; Ai, B. ADMM Based Channel Estimation for RISs Aided Millimeter Wave Communications. *IEEE Commun. Lett.* **2021**, *25*, 2894–2898. [[CrossRef](#)]
48. Li, S.; Duo, B.; Renzo, M.D.; Tao, M.; Yuan, X. Robust Secure UAV Communications With the Aid of Reconfigurable Intelligent Surfaces. *IEEE Trans. Wirel. Commun.* **2021**, *20*, 6402–6417. [[CrossRef](#)]
49. Yuan, J.; Liang, Y.-C.; Joung, J.; Feng, G.; Larsson, E.G. Intelligent Reflecting Surface-Assisted Cognitive Radio System. *IEEE Trans. Commun.* **2021**, *69*, 675–687. [[CrossRef](#)]
50. Zhou, G.; Pan, C.; Ren, H.; Wang, K.; Peng, Z. Secure Wireless Communication in RIS-Aided MISO System with Hardware Impairments. *IEEE Wirel. Commun. Lett.* **2021**, *10*, 1309–1313. [[CrossRef](#)]
51. Chen, Q.; Li, M.; Yang, X.; Alturki, R.; Alshehri, M.D.; Khan, F. Impact of Residual Hardware Impairment on the IoT Secrecy Performance of RIS-Assisted NOMA Networks. *IEEE Access* **2021**, *9*, 42583–42592. [[CrossRef](#)]
52. Zhou, S.; Xu, W.; Wang, K.; Renzo, M.D.; Alouini, M.-S. Spectral and Energy Efficiency of IRS-Assisted MISO Communication With Hardware Impairments. *IEEE Wirel. Commun. Lett.* **2020**, *9*, 1366–1369. [[CrossRef](#)]
53. Shen, H.; Xu, W.; Gong, S.; Zhao, C.; Ng, D.W.K. Beamforming Optimization for IRS-Aided Communications with Transceiver Hardware Impairments. *IEEE Trans. Commun.* **2021**, *69*, 1214–1227. [[CrossRef](#)]
54. Dayo, Z.A.; Cao, Q.; Wang, Y.; Pirbhulal, S.; Sodhro, A.H. A compact high-gain coplanar waveguide-fed antenna for military RADAR applications. *Int. J. Antennas Propag.* **2020**, *2020*, 8024101. [[CrossRef](#)]
55. Lakhan, A.; Dootio, M.A.; Groenli, T.M.; Sodhro, A.H.; Khokhar, M.S. Multi-Layer Latency Aware Workload Assignment of E-Transport IoT Applications in Mobile Sensors Cloudlet Cloud Networks. *Electronics* **2021**, *10*, 1719. [[CrossRef](#)]
56. Li, J.; Matthaiou, M.; Svensson, T. I/Q Imbalance in AF DualHop Relaying: Performance Analysis in Nakagami-m Fading. *IEEE Trans. Commun.* **2014**, *62*, 836–847. [[CrossRef](#)]
57. Li, X.; Zhao, M.; Gao, X.C.; Li, L.; Do, D.T.; Rabie, K.M.; Kharel, R. Physical Layer Security of Cooperative NOMA for IoT Networks under I/Q Imbalance. *IEEE Access* **2020**, *8*, 51189–51199. [[CrossRef](#)]
58. Yang, L.; Yang, Y.; Hasna, M.O.; Alouini, M.-S. Coverage, Probability of SNR Gain, and DOR Analysis of RIS-Aided Communication Systems. *IEEE Wire. Commu. Lett.* **2020**, *9*, 1268–1272. [[CrossRef](#)]
59. Basar, E.; Renzo, M.D.; Rosny, J.D.; Debbah, M.; Alouini, M.S.; Zhang, R. Wireless communications through reconfigurable intelligent surfaces. *IEEE Access* **2019**, *7*, 116753–116773. [[CrossRef](#)]
60. Gradshteyn, I.S.; Ryzhik, I.M. *Table of Integrals, Series, and Products*, 7th ed.; Academic: San Diego, CA, USA, 2007.
61. Kapinas, V.M.; Mihos, S.K.; Karagiannidis, G.K. On the monotonicity of the meneralized Marcum and Nuttall Q-functions. *IEEE Trans. Inf. Theory* **2009**, *55*, 3701–3710. [[CrossRef](#)]
62. Yang, L.; Meng, F.; Wu, Q.; da Costa, D.B.; Alouini, M.-S. Accurate Closed-Form Approximations to Channel Distributions of RIS-Aided Wireless Systems. *IEEE Wirel. Commu. Lett.* **2020**, *9*, 1985–1989. [[CrossRef](#)]
63. Peppas, K.P. Accurate closed-form approximations to generalised-K sum distributions and applications in the performance analysis of equal-gain combining receivers. *IET Commun.* **2011**, *5*, 982–989. [[CrossRef](#)]
64. Yang, L.; Yang, Y.; da Costa, D.B.; Trigui, I. Outage Probability and Capacity Scaling Law of Multiple RIS-Aided Networks. *IEEE Wirel. Commu. Lett.* **2021**, *10*, 256–260. [[CrossRef](#)]